Lasers in Eng., Vol. 46, pp. 367–381
Reprints available directly from the publisher
Photocopying permitted by license only

Ultrafast Laser Drilling of Crack-free, Debris-free and Heat Affected Zone (HAZ)-free Blind Holes in Al_2O_3 with Flat Bottom and Reduced Taper Angles

Z-L. LI[1], O. ALLEGRE[1], W. GUO[1], W-Y. GAO[2], B-H. LI[2], Q-L. FENG[2], X-P. WU[2] AND L. LI[1,*]

[1]*Laser Processing Research Centre, Department of Mechanical, Aerospace and Civil Engineering, The University of Manchester, Oxford Road, Manchester, M13 9PL, UK*
[2]*Beijing Institute of Aerospace Control Devices, 52 Yongdong Road, Beijing 100039, China*

Laser drilling of blind holes in materials often results in tapering and pointed bottom due to inappropriate beam intensity distribution, beam geometry, beam focal position and material flow erosions. In this work the effect of polarization states on taper angle at different focal plane position was analysed. A new approach of using a spatial filter shaped Gaussian laser beam from a Ti:Sapphire femtosecond laser was introduced to control the taper in the laser drilling of blind holes in Al_2O_3 ceramic sheets. Low taper angles and flat bottom blind holes were demonstrated drilled with the femtosecond laser and the holes were free from microcracks, recast layer, debris and without obvious heat affected zone (HAZ).

Keywords: Ti:Sapphire femtosecond laser, alumina ceramic, Al_2O_3, laser drilling, blind hole, trepanning, taper angle, microcracks, recast layer, debris, spatter heat affected zone (HAZ)

1 INTRODUCTION

Al_2O_3 alumina ceramic is a polycrystalline material with high hardness of 15 to 19 GPa, high electrical resistance of volume resistivity 10^{14} to 10^{15} Ωcm,

*Corresponding author: E-mail: lin.li@manchester.ac.uk

high dielectric strength in the region of 10 kV/mm, high corrosion and wear resistance, moderate thermal conductivity of 20 to 30 W/mK, very good chemical stability, low density of 3.75 to 3.95 g/cm^3, excellent mechanical strength of 300 to 630 MPa and high compressive strength of 2 to 4 GPa [1-6]. Al_2O_3 ceramic is widely applied in the microelectronics industry where scribing [7], *via* hole drilling [8] are required for the production of high temperature circuits, high power radio frequency electronic circuits, multichip modules and micro-electromechanical systems (MEMS) [9].

Mechanical methods for drilling Al_2O_3 include punching [6], stamping [10], broaching [11] and laser assisted machining (LAM) [12]. An advantage of these methods is that holes with large diameters can be drilled with low equipment cost. The disadvantages are extensive tool wear, surface and subsurface microcracks generation, residual stress generation and low efficiency [13]. Additionally, for drilling diameters smaller than a few hundred micrometers it becomes very difficult for mechanical drilling, often resulting in tool breakages. For ceramic materials with a high degree of brittleness or hardness the cutting forces would induce vibrations and may lead to material subsurface damages [6].

Several advanced drilling methods have been developed recently to overcome the challenges in mechanical drilling. Electrical discharge machining (EDM) [14] can achieve large depth drilling with a zero taper, and the equipment cost is low; however, the processing rate is very low, and it is also mainly suitable to machining of electrically conductive materials, although drilling non-conductive materials is possible [15]. With electrochemical machining (ECM) [16], excellent surfaces can be obtained, but the precision and efficiency [17] are difficult to be guaranteed for small holes. Also, it is not suitable for generating sharp corners due to the corrosive of electrolyte [18]. Photoetching [19], abrasive water jet cutting [20] and ultrasonic machining (USM) [21] have also been demonstrated for ceramic drilling and machining. Photo-etching is very slow, suitable for shallow holes only. Water jet cutting and ultrasonic drilling are not suitable for drilling precision micrometre-scale holes.

As a non-contact machining technology, laser beam machining (LBM) has been widely applied in industry [13, 22, 23]. For ceramic material machining photon energy is converted to thermal energy to raise the material temperature above the melting and/or vaporization temperatures. Since the reacting mechanical force is very low, material clamping is often not unnecessary. By processing in air or liquid [24, 25], high processing rate, high accuracy machining can be realised [26]. For high quality drilling of Al_2O_3, taper angle of the holes could be reduced or even changed from positive to negative in through hole drilling using long (millisecond) or short (nanosecond) pulse length lasers. For drilling Al_2O_3, however, there is a risk of cracks generation due to the thermal stresses, and the generation of a resolidified layer reduces the hole quality and durability of the holes [11]. Another method to reduce

the taper angle is to adjust the laser beam entrance angle in synchronizing with the trepanning motion. The drawback is that the system is very expensive, and the alignment and maintenance are quite difficult [27]. For laser blind hole drilling, taper free is still difficult to realize [27].

Continuous wave (CW) laser and long pulse length laser beams have been applied for achieving deep cavity machining and striation-free cutting of Al_2O_3 [28, 29]. Over the laser two decades ultrashort pulse (picosecond or femtosecond pulse duration) laser beams [30, 31] have become more used for high quality micro-scale ceramic drilling [32]. With the ultrashort pulse duration, the peak power intensity is over several GW/cm^2 and the laser beam can be effectively coupled to wide bandgap materials with multiphoton absorption (MPA) [10]. Since material removal is mainly based on evaporation, the residual heat affected zone (HAZ) and melting are minimised, and the edge quality can be improved [33,34]. By optimizing the laser parameters such as pulse duration, repetition rate, pulse energy, and focal plane position, drilling quality factors such as circularity, taper angle, HAZ, cracks, recast layer (spatter) and debris can be controlled [23, 34, 35]; for example, precise hole drilling on human dental dentine with well defined geometry haven been demonstrated [36, 37]. But until now, drilling Al_2O_3 blind holes with vertical hole walls and flat bottom is still difficult to achieve even with an ultrafast laser at picosecond or femtosecond pulses.

In this paper, an investigation into achieving high quality flat bottom blind hole drilling on Al_2O_3 sheets with reduced taper using a Ti:Sapphire femtosecond laser in air is reported. Beam polarization states such as linear, circular, radial, and azimuthal polarization were studied in the drilling blind holes in alumina ceramic by fill trepanning. The quality of the hole including taper angle, and surface roughness was analysed. Blind holes with low taper angles, free from HAZ, cracks, recast layer, and debris and with a flat bottom were achieved.

2 EXPERIMENTAL PROCEDURES

A Ti:Sapphire femtosecond laser (Libra Ti:Sapphire; Coherent, Inc.) was used at an 800 nm wavelength with a 100 femtosecond pulse duration, a 1 kHz repetition rate, M^2 smaller than 1.5, an output power of up to 1 W, with an approximately Gaussian beam intensity distribution and a raw beam diameter of 5 mm. Neutral density filters and a polarization attenuator were applied to controlling the pulse energy. A quarter waveplate (WPQ10ME-780; Thorlabs, Inc.) and a s-waveplate (RPC-800-08; Altechna) were applied to transforming linear polarization to circular polarization or radial/azimuthal polarization. After several 45^o reflections from several low-group-delay-dispersion, thin-film-coated ultrafast mirrors, the laser beam was directed to an *x-y* scanning galvanometer and focused through a f-theta lens with a 100 mm focal length.

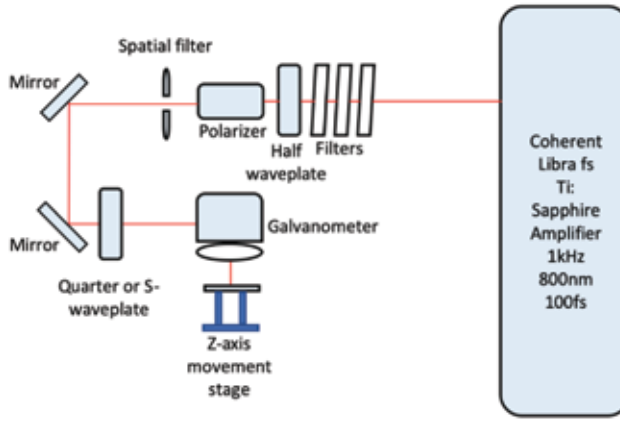

FIGURE 1
Schematic diagram of the femtosecond laser beam path arrangement.

An Al_2O_3 alumina ceramic sheet with a 1 mm thickness was placed on a vertical (z-axis) translation stage. The femtosecond laser beam path arrangement is shown in Figure 1. The diameter of the focused laser beam and depth of focus were calculated to be 30.6 μm in $1/e^2$ and 1.22 mm, respectively, based on [38, 39]

$$d_{\min} = \frac{4M^2\lambda f}{\pi D_L} \tag{1}$$

and

$$Z_F = \frac{8M^2\lambda f^2}{\pi D_L{}^2} \tag{2}$$

where M^2=1.5 is the beam quality factor, λ is the wavelength, f is the focal length and D_L is the raw beam diameter. In the infrared (IR) wavelength spectrum, Al_2O_3 has a strong absorption [40]. The ablation threshold fluence was estimated with the method described previously [10, 41] to be around 1.28 J/cm^2. The common laser drilling methods are single pulse drilling [13], percussion [42], trepanning [35] and helical drilling [43]. In this work a fill trepanning method of multiple centric rings or loops, as shown illustrated in Figure 2, with linear, circular, radial or azimuthal polarization states was applied.

The effect drilling two pieces of Al_2O_3 were attached together. The laser beam was focused at the boundary area of the two samples. The cross-section

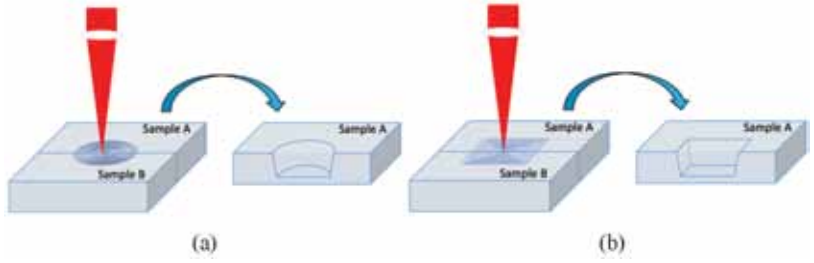

FIGURE 2
Schematic diagrams showing the laser beam filling trepanning regime for (a) circular hole and (b) square hole drilling.

drilling profile could be obtained in this way (see Figure 2) without having to cut the samples.

Sample analysis was conducted with a scanning electron microscope (SEM) (Ultra 55; Carl Zeiss AG). Before the samples were observed under the SEM a 10 nm thick Au/Pd coating was applied to make the surfaces conductive. The sidewall quality was analysed with a white light interferometer (WLI) (Contour GT-K; Veeco Instruments, Inc.) and an optical microscope (VHX 5000; Keyence Corporation).

3 RESULTS AND DISCUSSION

3.1 Effect of beam polarization states on hole circularity

A comparison of the drilling results with different polarization states was carried out. After twice reflections inside the scanning galvanometer, the polarization state was rotated counter-clockwise by 27° relative to the original laser beam polarization direction. The results were normalized to be a linear polarization direction. In the beam path, circular polarization could be conversed by using a quarter waveplate. Radial and azimuthal polarization could be generated by using a s-waveplate. Through hole drilling of the Al_2O_3 plate was carried out for examining the circularity on the exit hole. During the drilling the focal plane was placed on the top surface of the material, setting the expected hole diameter, pulse energy, scanning speed, hatching distance and processing passes to be 1 mm, 300 μJ, 10 mm/s, 10 μm and 80 passes respectively, each pass took around 2.1 seconds. On the hole entrance side (see Figures 3(a) to (d)) the circularity for all polarizations was close to 1, and the diameters were almost the same, which was around 970 μm. In Figures 3(a) to (d) the shadows show the tapering of the thorough hole holes, rather than HAZ or recast. On the hole exit side (see Figures 3(e) to (h)) the circularity for the linear, circular, radial and azi-

TABLE 1
Circularity calculation for through hole drilling by using four polarization states.

Polarizations State	Hole Entrance		Hole Exit	
	Diameter (μm)	Circularity	Diameter (μm)	Circularity
Linear polarization	975 - 973	0.998	409 - 540	0.757
Circular polarization	966 - 965	0.999	549 - 550	0.998
Radial polarization	973 - 970	0.997	510 - 564	0.904
Azimuthal polarization	971 - 967	0.996	514 - 564	0.911

muthal polarization states were 0.757, 0.998, 0.904, and 0.911, respectively, (*cf.* Table 1), based on [44]

$$C = \frac{D_{\min}}{D_{\max}} \tag{3}$$

where C is the circularity, $D_{\min}$ is the minimum hole diameter and $D_{\max}$ is the maximum hole diameter. This was consistent with the principle that for linear polarization, the laser material interaction in the regions where *p*-polarization dominates would be enhanced [45], so that the hole exit would be elongated to the direction of polarization, which reduced the drilling circularity; therefore, circular, radial and azimuthal polarization states were more suitable for the high quality drilling of the ceramic material. Tapering was present in all the holes drilled as the entrance hole diameters were larger than the exit hole diameters and the exit hole diameters were generally smaller and irregular. For circular polarized beam, hole symmetry is better, because of its isotropic properties [46]. From Figure 3(g) it is clear that the holes are free from any debris and spatter.

3.2 Focal plane position effect on taper angle

To study the focal plane position effect, the focal plane was placed above the top surface (+1 mm), on the top surface (0 mm) and below the top surface (-1 mm, -2 mm) of the Al_2O_3 respectively. With 20 and 40 passes scanning, depth and taper angle were measured and analysed as shown in Figure 4 and Figure 5.

It can be s that scanning passes did not affect taper angle much. The smallest taper angle was achieved when placing the focal plane 1 mm below the top surface of the sample for all three polarization states. This is because by lowering the focal plane, more pulse energy could be delivered into low part of the hole. By comparing circular polarization results with radial and azimuthal polarization, the taper angle was larger in the former situation when the focal plane was on the top surface. This was probably due to the laser beam with a radial or azimuthal polarization having a polarization singularity

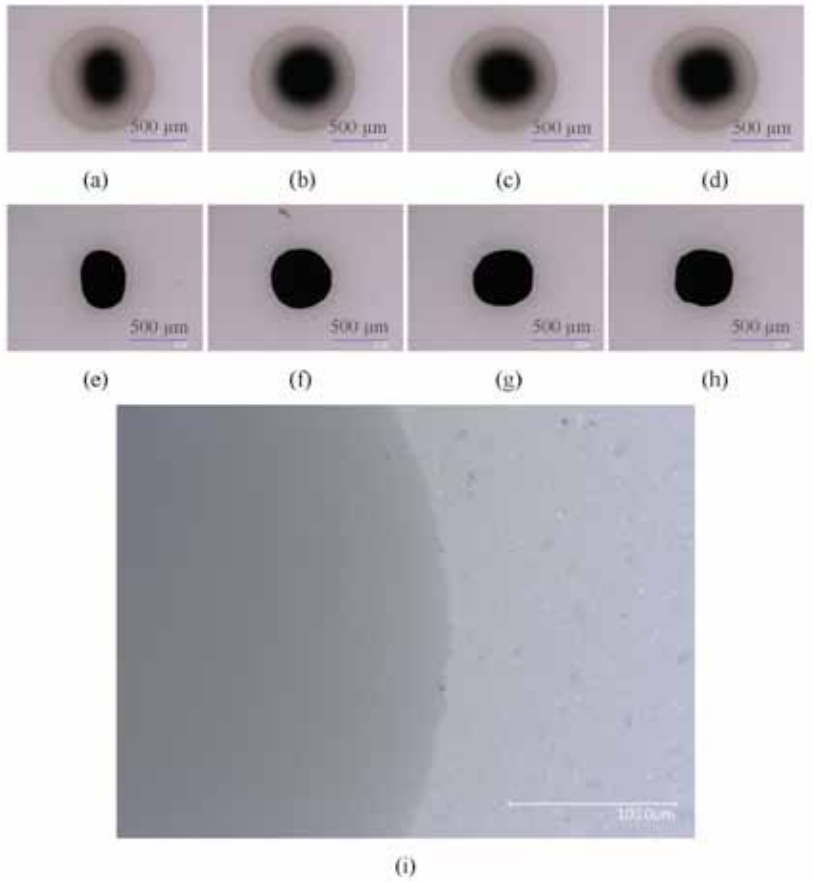

FIGURE 3
SEM micrographs showing typical through hole drilling hole geometry in the 1 mm thick Al_2O_3 for (a) the top surface drilled with a linear polarized beam,(b) the top surface drilled with a circular polarized beam, (c) the top surface drilled with a radially polarized beam, (d) the top surface drilled with an azimuthal polarized beam, (e) the bottom surface drilled with a linear polarized beam, (f) the bottom surface drilled with a circular polarized beam, (g) the bottom surface drilled with a radial polarized beam, (h) bottom surface drilled with an azimuthal polarized beam and (i) the enlarged hole entrance edge.

in the centre of the beam, which made it an annular intensity distribution, as shown in Figure 5.

By examining the depth of drilling with the three polarization states, 40 passes scanning resulted in almost the twice depth of 20 passes. In the 40 passes scanning, The deepest drilling can be obtained by placing the focal plane on the top surface. When moving the focal plane from the sample surface to 1 mm below, it was found that the taper angle was reduced and depth

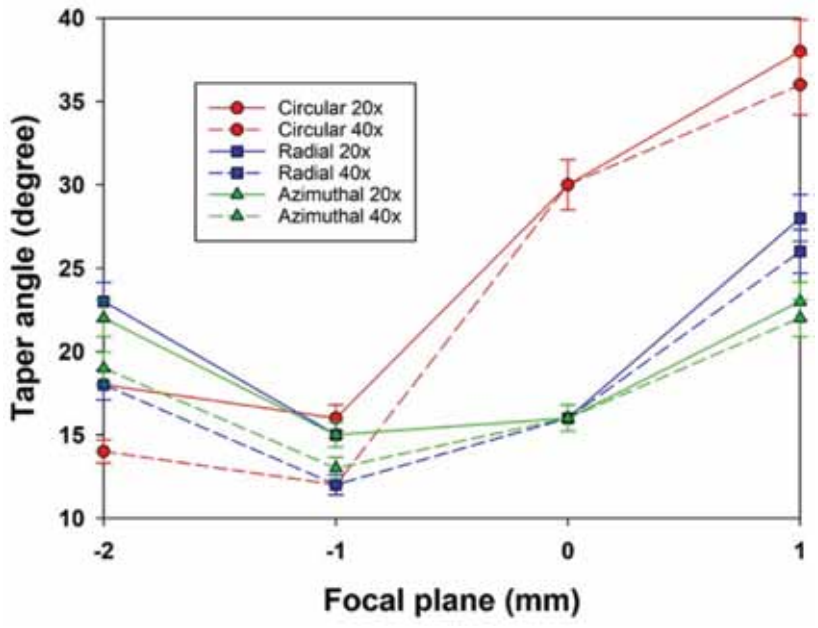

FIGURE 4
Graph showing the change in taper angle with focal plane.

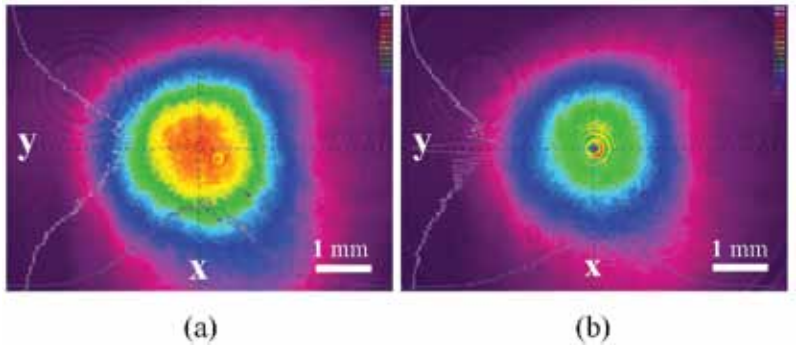

FIGURE 5
Femtosecond laser beam profiles with (a) linear or circular polarization states and (b) radial or azimuthal polarization states.

was reduced as well. It means that in this situation, some pulse energy was lost to the side walls.

3.3 Effect of laser beam intensity distribution

The laser beam was not a perfect Gaussian beam profile. A spatial filter was used to optimise the Gaussian beam to be more circular. This was realised by

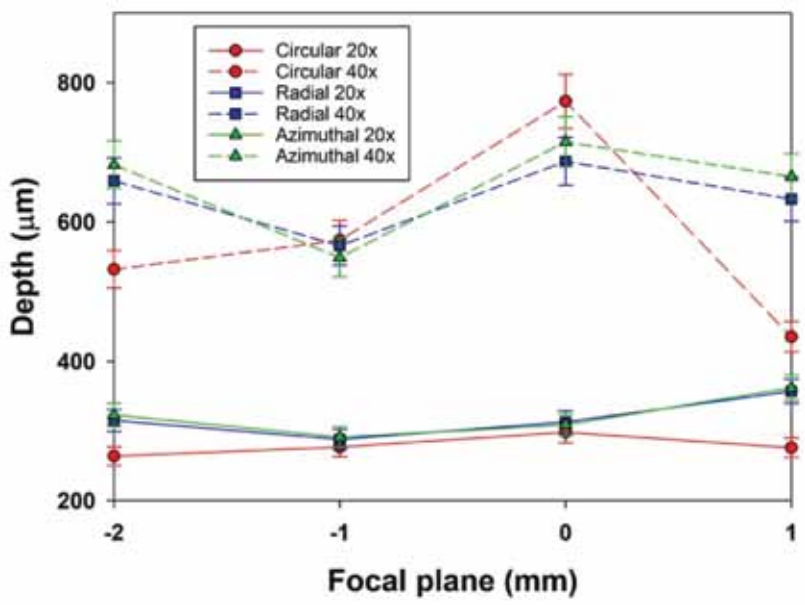

FIGURE 6
Graph showing the effect of focal plane on the depth of drilling.

placing an aperture in the beam path. By reducing the aperture diameter, the Gaussian beam would be partially blocked, leaving the central area where the intensity distribution was more uniform. The aperture diameters of 5, 4, 3 and 2 mm were used. The resulting beam profiles are shown in Figure 7.

By placing the sample surface relative to focal plane and applying the circular using circular polarization, at 170 μJ pulse energy, 10 mm/s scanning speed, 500 μm scanning diameter and 10 μm hatching distance with 45 passes, and fill-trepanning was used, the results are shown in Figure 8. It can be seen from Figure 8 that when the aperture diameter of the spatial filter was reduced to 4 mm, the smallest taper angle could be obtained. This may be due to the spatial filter generated interference patterns (as shown in

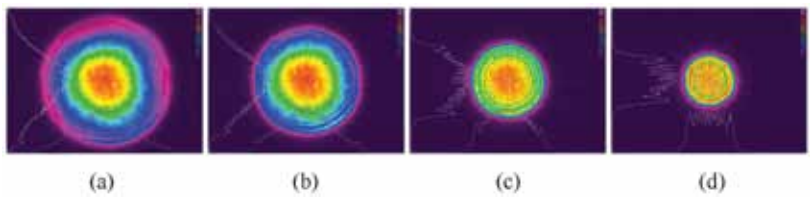

FIGURE 7
Femtosecond laser beam profiles with different aperture sizes for the original Gaussian beam, spatial filter shaped beam with a diameter of (a) 5 mm, (b) 4 mm, (c) 3 mm and (d) 2 mm.

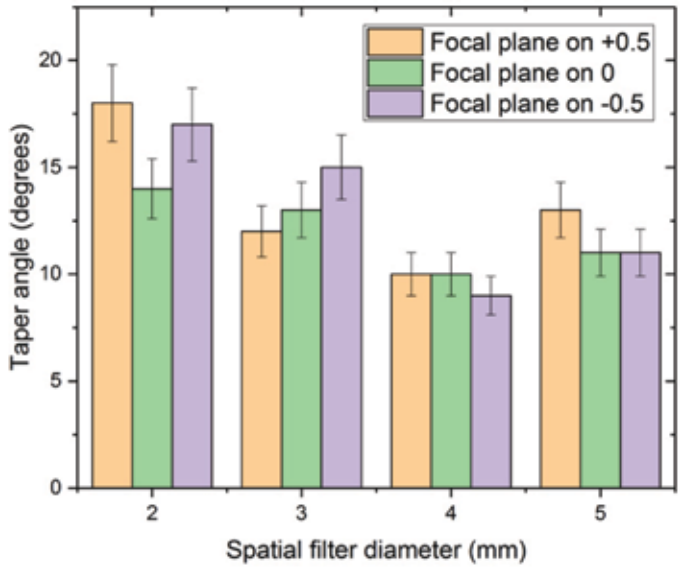

FIGURE 8
Bar chart showing the effect of femtosecond laser beam diameter and focal plane position on the hole taper.

Figure 7(b)). The laser beam focusing through the f-theta lens had a more uniform intensity distribution and the laser material interaction angle became larger so that the taper angle was reduced. Further reducing the beam diameter, the focal spot size would become larger, reducing the beam intensity.

3.4 Blind hole characteristics

The cross-section of a blind hole generated by placing the focal plane 1 mm below top surface is shown in Figure 8. High quality drilling with no HAZ, cracks, recast layer or debris was achieved. For a 500 μm diameter blind hole laser drilling, a taper angle would be generated from the first scanning of fill-trepanning. With the following scanning passes, the hole became deeper. Based on the observation of Figure 8, and the data from Figure 4, with the increase of the scanning passes from 20 to 40, taper angle was reduced by around 25, 20 and 13% for circular, radial and azimuthal polarization states respectively. Further increase in the scanning passes, a pointed bottom would be generated.

To create a blind hole with reduced taper, focal plane below the top surface of material by 1 mm was selected. With the circular polarization, the raw beam diameter was reduced into 4 mm. Under 220 μJ and 20 scanning passes was conducted. The generated blind hole as shown in Figure 9. After 20 scanning passes, the focal plane was downward shifted by 200 μm, and carried out

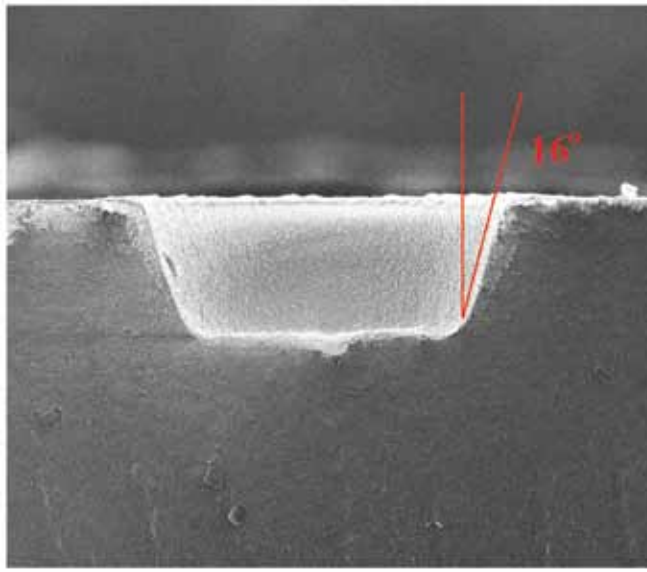

FIGURE 9
SEM micrograph of a blind hole in the Al_2O_3 after the first 20 scanning passes of the femtosecond laser beam.

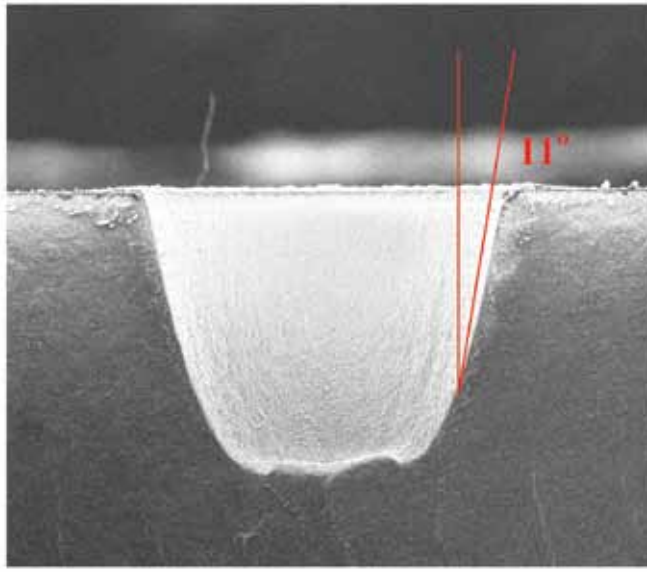

FIGURE 10
SEM micrograph of a blind hole in the Al_2O_3 after the second 20 scanning passes of the femtosecond laser beam.

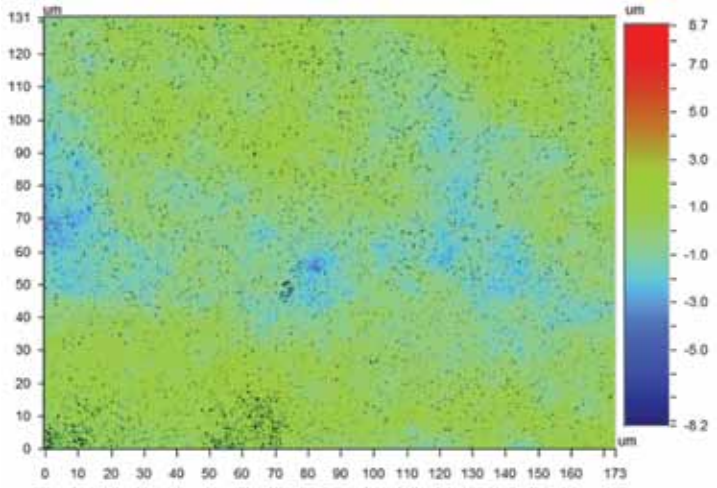

FIGURE 11
WLI roughness measurements on the bottom of a blind hole.

another 20 scanning passes. From Figure 10 the taper angle was further reduced. By WLI the measured roughness on the bottom of blind hole was around 0.8 μm Ra, as shown in Figure 11.

4 CONCLUSIONS

Fill-trepanning was applied for drilling blind holes in Al_2O_3 alumina ceramic using a Ti:Sapphire femtosecond laser. By comparing linear, circular, radial and azimuthal polarization states, and the effect of focal plane position, it was found that radial and azimuthal polarization were better for reducing taper due to its special beam intensity distribution. A spatial filter was used to reduce the raw beam diameter, and the special intensity distribution helps to reduce the taper angle, especially when the focal plane was placed 1 mm below the top surface. Based on the optimized parameters, low taper angle blind hole with a flat bottom were processed without microcracks, recast layer, debris (spatter) or a discernible heat affected zone (HAZ).

ACKNOWLEDGMENT

This research was partially supported by the National Key R&D Program of China (2017YFB1104604).

NOMENCLATURE

C	Circularity
D_L	Raw beam diameter (m)
$d_{\min}$	Diameter of the focused laser beam (m)
$D_{\min}$	Minimum hole diameter (m)
$D_{\max}$	Maximum hole diameter (m)
f	focal length of the lens (m)
Z_F	Depth of focus (m)

Greek symbol

λ	Wavelength of laser beam (m)

REFERENCES

[1] Hu P. and Wang Z. Flexural strength and fracture behavior of ZrB_2–SiC ultra-high temperature ceramic composites at 1800°C. *Journal of the European Ceramic Society* **30**(4) (2010), 1021–1026.

[2] Zou B., Huang C., Song J., Liu Z., Liu L. and Zhao Y. Mechanical properties and microstructure of TiB2–TiC composite ceramic cutting tool material. *International Journal of Refractory Metals and Hard Materials* **35** (2012), 1–9.

[3] Huang S.G., Vanmeensel K., Malek O.J.A., Van der Biest O. and Vleugels J. Microstructure and mechanical properties of pulsed electric current sintered B_4C–TiB_2 composites. *Materials Science & Engineering A. Structural Materials: Properties, Microstructure and Processing* **528**(3) (2011), 1302–1309.

[4] Peillon F.C. and Thevenot F. Microstructural designing of silicon nitride related to toughness. *Journal of the European Ceramic Society* **22**(3) (2002), 271–278.

[5] Shi J.L., Li B.S. and Yen T.S. Mechanical properties of Al_2O_3 particle-Y-TZP matrix composite and its toughening mechanism. *Journal of Materials Science* **28**(15) (1993), 4019–4022.

[6] Wang X.C., Zheng H.Y., Chu P.L., Tan J.L., Teh K.M., Liu T., Ang B.C.Y. and Tay G.H. Femtosecond laser drilling of alumina ceramic substrates. *Applied Physics A: Materials Science & Processing* **101**(2) (2010), 271-278.

[7] Lumpp J.K. and Allen S.D. Excimer laser machining and metallization of vias in aluminum nitride. *IEEE Transactions on Components, Packaging and Manufacturing Technology B* **20**(3) (1997), 241-246.

[8] Li C., Lee S. and Nikumb S. Femtosecond laser drilling of alumina wafers. *Journal of Electronic Materials* **38**(9) (2009), 2006–2012.

[9] Yu Z.Y., Zhang Y., Li J., Luan J., Zhao F. and Guo D. High aspect ratio micro-hole drilling aided with ultrasonic vibration and planetary movement of electrode by micro-EDM. *CIRP Annals* **58**(1) (2009), 213–216.

[10] Perrie W., Rushton A., Gill M., Fox P. and O'Neill W. Femtosecond laser micro-structuring of alumina ceramic. *Applied Surface Science* **248**(1) (2005), 213–217.

[11] Kacar E., Mutlu M., Akman E., Demir A., Candan L., Canel T., Gunay V. and Sınmazcelik T. Characterization of the drilling alumina ceramic using Nd:YAG pulsed laser. *Journal of Materials Processing Technology* **209**(4) (2009), 2008–2014.

[12] Kumar M., Melkote S. and Lahoti G. Laser-assisted microgrinding of ceramics. *CIRP Annals* **60**(1) (2011), 367–370.

[13] Sushant D., Nishant S. and Purohit R. A review on laser drilling and its techniques. *International Conference on Advances in Mechanical Engineering (AME 2006)*. 1-3 December 2006. Fatehgarh Sahib, India. pp. 77-96.

[14] Diver C., Atkinson J., Helml H.J. and Li L. Micro-EDM drilling of tapered holes for industrial applications. *Journal of Materials Processing Technology* **149**(1-3) (2004), 296–303.
[15] Puertas I. and Luis C.J. A study on the electrical discharge machining of conductive ceramics. *Journal of Materials Processing Technology* **153-154** (2004), 1033–1038.
[16] Park B.J., Kim B.H. and Chu C.C. The effects of tool electrode size on characteristics of micro electrochemical machining. *CIRP Annals* **55**(1) (2006), 197-200.
[17] Chak S.K. and Venkateswara Rao P. Trepanning of Al_2O_3 by electro-chemical discharge machining (ECDM) process using abrasive electrode with pulsed DC supply. *International Journal of Machine Tools and Manufacture* **47**(14) (2007), 2061–2070.
[18] Hanon M.M., Akman E., Genc Oztoprak B., Gunes M., Taha Z.A., Hajim K.I., Kacar E., Gundogdu O. and Demir A. Experimental and theoretical investigation of the drilling of alumina ceramic using Nd:YAG pulsed laser. *Optics & Laser Technology* **44**(4) (2012), 913–922.
[19] Masuzawa T. State of the art of micromachining. *CIRP Annals* **49**(2) (2000), 473-488.
[20] Gudimetla P., Wang J., Wong W. Kerf formation analysis in the abrasive waterjet cutting of industrial ceramics. *Journal of Materials Processing Technology* **128**(1-3) (2002), 123-129.
[21] Li Z.C., Jiao Y., Deines T.W., Pei Z.J. and Treadwell C. Rotary ultrasonic machining of ceramic matrix composites: feasibility study and designed experiments. *International Journal of Machine Tools and Manufacture* **45**(12-13) (2005), 1402–1411.
[22] Corcoran A., Sexton L., Seaman B., Ryan P. The laser drilling of multi-layer aerospace material systems. *Journal of Materials Processing Technology* **123**(1) (2002), 100-106.
[23] Wang H., Lin H., Wang C., Zheng L. and Hu X. Laser drilling of structural ceramics—A review. *Journal of the European Ceramic* Society **37**(4) (2017), 1157–1173.
[24] Li C., Shi X., Si J., Chen T., Chen F., Liang S., Wu Z. and Hou X. Alcohol-assisted photoetching of silicon carbide with a femtosecond laser. *Optics Communications* **282**(1) (2009), 78–80.
[25] Iwatani N., Doan H.D. and Fushinobu K. Optimization of near-infrared laser drilling of silicon carbide under water. *International Journal of Heat and Mass Transfer* **71** (2014), 515–520.
[26] Samant A.N. and Dahotre N.B. Laser machining of structural ceramics - A review. *Journal of the European Ceramic Society* **29**(6) (2009), 969–993.
[27] Jahns D., Kaszemeikat T., Mueller N., Ashkenasi D., Dietrich R. and Eichler H.J. Laser trepanning of stainless steel. *Physics Procedia* **41** (2013), 630–635.
[28] Yan Y., Li L., Sezer K., Wang W., Whitehead D., Ji L., Bao Y. and Jiang Y. CO_2 laser underwater machining of deep cavities in alumina. *Journal of the European Ceramic Society* **31**(15) (2011), 2793–2807.
[29] Yan Y., Li L., Sezer K., Whitehead D., Ji L., Bao Y. and Jiang Y. Nano-second pulsed DPSS Nd:YAG laser striation-free cutting of alumina sheets. *International Journal of Machine Tools and Manufacture* **53**(1) (2012), 15–26.
[30] Hirayama Y., Yabe H. and Obara M. Selective ablation of AlN ceramic using femtosecond, nanosecond, and microsecond pulsed laser. *Journal of Applied Physics* **89**(5) (2001), 2943–2949.
[31] Kononenko T.V., Klimentov S.M., Garnov S.V., Konov V.I., Breitling D., Foehl C., Ruf A., Radtke J. and Dausinger F. Hole formation process in laser deep drilling with short and ultrashort pulses. *Second International Symposium on Laser Precision Micromachining (SPIE 2001)*. 25 February 2002, Singapore. **4426**, pp. 108–112.
[32] Qin Y., Brockett A., Ma Y., Razali A., Zhao J., Harrison C., Pan W., Dai X. and Loziak D. Micro-manufacturing: research, technology outcomes and development issues. *International Journal of Advanced Manufacturing Technology* **47**(9-12) (2009), 821–837.
[33] Chen X. and Liu X. Short pulsed laser machining: How short is short enough? *Journal of Laser Applications* **11**(6) (1999), 268–272.
[34] Mishra S. and Yadava V. Laser beam micromachining (LBMM) - A review. *Optics and Lasers in Engineering* **73** (2015), 89–122.

[35] Yilbas B.S., Akhtar S.S. and Karatas C. Laser trepanning of a small diameter hole in titanium alloy: Temperature and stress fields. *Journal of Materials Processing Technology* **211**(7) (2011), 1296–1304.

[36] Ji L., Li L., Devlin H., Liu Z., Jiao J. and Whitehead D. Ti:sapphire femtosecond laser ablation of dental enamel, dentine, and cementum. *Lasers in Medical Science* **27**(1) (2012), 197–204.

[37] Ji L., Li L. Devlin H., Liu Z., Whitehead D., Wang Z. Wang W. and Jiao J. Effect of different processing parameters of Ti: Sapphire femtosecond laser on human dental dentine. *36th International MATADOR Conference*. 14-16 July 2010, Manchester, UK. pp. 473-476.

[38] Harp W.R., Paleocrassas A.G. and Tu J.F. A practical method for determining the beam profile near the focal spot. *International Journal of Advanced Manufacturing Technology* **37**(11-12) (2007), 1113–1119.

[39] Steen W.M. and Mazumder J. *Laser Material Processing*. Berlin: Springer. 2010.

[40] Radtke J., Abeln T., Weikert M. and Dausinger F. High-precision microcutting of ceramics with short-pulsed solid state lasers. *First International Symposium on Laser Precision Microfabrication (LMP 2000)*. 6 November 2000, Omiya, Saitama, Japan. **4088**, pp. 252–255.

[41] Lawrence J. and Li L. Determination of the absorption length of CO_2 and high power diode laser radiation for a high volume alumina-based refractory material. *Applied Surface Science* **168**(1-4) (2000), 71-74.

[42] Yan Y., Ji L., Bao Y. and Jiang Y. An experimental and numerical study on laser percussion drilling of thick-section alumina. *Journal of Materials Processing Technology* **212**(6) (2012), 1257–1270.

[43] Fornaroli C., Holtkamp J. and Gillner A. Laser-beam helical drilling of high quality micro holes. *Physics Procedia* **41** (2013), 661–669.

[44] Chatterjee S., Mahapatra S.S., Bharadwaj V., Choubey A., Upadhyay B.N. and Bindra K.S. Drilling of micro-holes on titanium alloy using pulsed Nd:YAG laser: Parametric appraisal and prediction of performance characteristics. *Proceedings of the Institution of Mechanical Engineers, Part B: Journal of Engineering Manufacture* **233**(8) (2018), 1872–1889.

[45] Allegre O.J., Li Z. and Li L. Tailored laser vector fields for high-precision micro-manufacturing. *CIRP Annals* **68**(1) (2019), 193–196.

[46] Nolte S., Momma C., Kamlage G., Ostendorf A., Fallnich C., Von Alvensleben F. and Welling H. Polarization effects in ultrashort-pulse laser drilling. *Applied Physics A: Materials Science & Processing* **68**(5) (1999), 563-567.